Author/s:
Policheni, A;Horikawa, K;Milla, L;Kofler, J;Bouillet, P;Belz, GT;O'Reilly, LA;Goodnow, CC;Strasser, A;Gray, DHD

Title:
CARD11 is dispensable for homeostatic responses and suppressive activity of peripherally induced FOXP3+ regulatory T cells

Date:
2019-09-01

Citation:
Policheni, A., Horikawa, K., Milla, L., Kofler, J., Bouillet, P., Belz, G. T., O'Reilly, L. A., Goodnow, C. C., Strasser, A. & Gray, D. H. D. (2019). CARD11 is dispensable for homeostatic responses and suppressive activity of peripherally induced FOXP3+ regulatory T cells. Immunology and Cell Biology, 97 (8), pp.740-752. https://doi.org/10.1111/imcb.12268.

ASSOCIATE PROFESSOR DANIEL GRAY (Orcid ID : 0000-0002-8457-8242)

Article type : Original Article

CARD11 is dispensable for homeostatic responses and suppressive activity of peripherally-induced FOXP3+ regulatory T cells

Antonia Policheni[1,2], Keisuke Horikawa[3], Liz Milla[1,2], Jennifer Kofler[3], Philippe Bouillet[1,2], Gabrielle T. Belz[1,2], Lorraine A. O'Reilly[1,2], Christopher C. Goodnow[4], Andreas Strasser[1,2], Daniel H.D. Gray[1,2,*]

[1] The Walter and Eliza Hall Institute of Medical Research, Parkville, Australia.

[2] Department of Medical Biology, The University of Melbourne, Parkville, Australia.

[3] Australian Cancer Research Foundation Department of Cancer Biology and Therapeutics, The John Curtin School of Medical Research, The Australian National University, Australia.

[4] Garvan Institute of Medical Research, Sydney, Australia.

* To whom correspondence should be addressed: dgray@wehi.edu.au

Keywords: Card11, regulatory T cells, homeostasis, mutant.

Running title: CARD11 and regulatory T cell homeostasis

Abstract (250 words)

FOXP3$^+$ regulatory T (Treg) cells are essential for immunological tolerance and immune homeostasis. Despite a great deal of interest in modulating their number and function for the treatment of autoimmune disease or cancer, the precise mechanisms that control the homeostasis of Treg cells remain unclear. We report a new ENU-induced mutant mouse, *loco*, with atopic dermatitis and Treg cell deficiency typical of *Card11* loss-of-function mutants. Three distinct single nucleotide variants were found in the *Card11* introns 2, 10 and 20 that cause the loss of CARD11 expression in these mutant mice. These mutations caused the loss of thymic-derived, NRP1$^+$ Treg cells in neonatal and adult *loco* mice, however residual peripherally-induced NRP1$^-$ Treg cells remained. These peripherally generated Treg cells could be expanded *in vivo* by administration of IL-2:anti-IL-2 complexes, indicating this key homeostatic signaling axis remained intact in CARD11-deficient Treg cells. Furthermore, these expanded Treg cells could mediate near normal suppression of activated, conventional CD4$^+$ T cells, suggesting that CARD11 is dispensable for Treg cell function. In addition to shedding light on the requirements for CARD11 in Treg cell homeostasis and function, these data reveal novel non-coding *Card11* loss-of-function mutations that impair expression of this critical immune-regulatory protein.

Introduction

FOXP3$^+$ regulatory T (Treg) cells are essential mediators of immunological tolerance and immune homeostasis. The critical role of this specialized T cell subset is highlighted by studies of *FOXP3*-deficiency that cause the auto-inflammatory IPEX syndrome in humans and the *scurfy* mutant mouse strain[1-4]. Furthermore, dysregulation of Treg cells has been linked to a variety of autoimmune pathologies[1, 4-7]. The primary function of Treg cells is to exert dominant tolerance on naïve T cells by keeping their activation in check or curtailing the function of effector T cells[8-10]. The potential to enlist the potent immunomodulatory properties of Treg cells for the treatment of immune disorders or suppress their activity to enhance immune responses against cancers has prompted great interest in the factors controlling their differentiation and homeostasis.

Treg cells are a mature subpopulation of CD4$^+$ T cells characterized by the expression of the transcription factor FOXP3 and the IL-2 receptor α chain, CD25[8, 11]. Most Treg cells are

produced in the thymus via three major signals: (1) the high avidity recognition of self-peptide:MHC complexes by the TCRα/β, (2) IL-2 (and, to a lesser extent, other cytokines that activate common gamma chain containing surface receptors) that supports their survival and further differentiation, and (3) signals from various TNFR family members in the thymic medulla[6, 12-16]. Treg cells can also be generated from mature $CD4^+$ T cells following TCR ligation under certain conditions, predominantly at mucosal locations[17]. The homeostatic mechanisms maintaining thymic and/or peripherally-induced Treg cells remain poorly understood. IL-2 remains critical for lymphoid Treg cell homeostasis *in vivo* and their expression of the high affinity form of the IL-2R allows them to outcompete conventional T cells for this critical cytokine[18]. Accordingly, administration of IL-2 complexed with antibodies that stabilize and target this cytokine to the high affinity IL-2R induces substantial expansion of Treg cells in mice[19]. TCR signals in the periphery are required for Treg cell activation, effector Treg cell differentiation and their recruitment into tissues to control inflammation[20, 21]. However, many outstanding questions remain about the integration of these signals and their interplay to control the development and function of different Treg cell populations.

CARD11 (also known as CARMA1) encodes a membrane-associated guanylate kinase (MAGUK) family protein that is essential for thymic Treg cell differentiation and lymphocyte activation[22]. Following T cell activation, protein kinase C phosphorylates CARD11 to enable its oligomerization and association with BCL10 and MALT1 to form the CBM complex, a scaffold required for activation of IκB (IKK) and nuclear factor-κB (NFκB) responses[23]. Treg cells exhibit a heightened requirement for c-REL, a member of the NF-κB transcription factor family, for their thymic differentiation compared to conventional T cells[8], perhaps providing an explanation for the increased importance of CBM signals for this cell population. The CBM has also been implicated in other signaling modalities important for Treg cells, for example signaling from the IL-2R[24], although other data would seem to contradict this notion [25]. Nevertheless, loss-of-function mutations in *Card11* result in primary immunodeficiency diseases, with the emergence of atopic dermatitis in some strains of *Card11* mutant mice and in human patients [26; 27]. Dermatitis in *Card11*-deficient mice has been linked to thymic Treg cell deficiency, with supplementation of wild-type (wt) Treg cells preventing disease[26]. In contrast, gain-of-function mutations in *Card11* have been linked to hyperproliferative B cell disease BENTA (B-cell

expansion with NF-kB and T cell anergy) in humans and are implicated in the development of B and T cell lymphomas, such as diffuse large B cell lymphoma, Sézary disease and adult T cell leukaemia/lymphoma [28].

Although extensive literature has reported important roles for CARD11 in immune pathologies, many open questions remain, including: what is the impact of *Card11* mutations directly on the capacity of peripherally-induced Treg cells to respond to homeostatic cues? Is CARD11 required for the suppressive activity of Treg cells? How is the expression of *Card11* regulated? These issues have relevance to our understanding of immunological tolerance and the basis of the immune pathologies observed with *Card11* mutations. Here, we investigated the role of CARD11 in Treg cell development, homeostasis and function with a new ENU mutant mouse model.

Results

A novel mutant mouse strain, loco, with Treg cell deficiency uncovered in a sensitized ENU mutagenesis screen

In order to discover novel immune tolerance genes, we conducted a forward genetic screen for phenotypes associated with autoimmunity. We employed the mutagen ethyl-nitrosourea[29] to introduce point mutations throughout the genome of the male germline cells of C57BL/6 mice. However, given the wealth of evidence that most autoimmune diseases are multigenic, involving defects in several different tolerance mechanisms, we also introduced a "sensitizer" allele. The *Vav-Bcl-2* transgene drives overexpression of the pro-survival protein BCL-2 in all hematopoietic cells[30] and these animals, similar to *Eμ-Bcl-2* transgenic mice, display signs of enhanced auto-reactivity of B cells, increased numbers of Ig class-switched B cells and peripheral T cells and are prone to autoimmune glomerulo-nephritis[31, 32]. This transgene was introduced into pedigrees established to screen for recessive traits that cooperate with defects in apoptosis to elicit autoimmune disease. Pedigrees of mice were screened for blood lymphocyte abnormalities by flow cytometry. One mutant strain, *loco*, (lack of co-stimulation) was identified due to a significant decrease in $CD4^+CD25^+$ Treg cells in the blood (**Figure 1a**). This phenotype was inherited as a fully penetrant recessive trait and was accompanied by a reduction of $CD19^+$

B cells (**Figure 1b**). Analysis of the B cell compartment of *loco* mice revealed altered expression of the B cell antigen receptors IgD and IgM (**Figure 1c**). With age, these mutant mice developed obvious signs of dermatitis (**Figure 1d**), with affected areas exhibiting epidermal hyperplasia (**Figure 1e)**. All *loco* mice analysed developed progressive dermatitis that necessitated euthanasia while no control mice succumbed to this disease over this period (**Figure 1f**). The development of dermatitis was accompanied by increased levels of serum IgE in loco mice (**Figure 1g**). No other signs of immune pathology were observed in other organs from *loco* mutant mice (**Supplementary Figure 1**).

Analysis of peripheral lymphoid organs for FOXP3 expression confirmed the loss of Treg cells in all major compartments (**Figure 1h-j**), while normal proportions of conventional $CD4^+$ T cells were found (**Supplementary Figure 2a**). T cell differentiation in the thymus from *loco* mutant mice appeared grossly normal, with normal proportions of CD4/CD8 double negative (DN), double positive (DP) and CD4 single positive (SP) and CD8SP thymocytes, and CD44/CD25 thymic progenitor subsets (**Figure 1i, Supplementary Figure 2b**). However, $FOXP3^+$ Treg cells were nearly completely absent from the thymus of the *loco* mutant mice and their $GITR^{high}CD25^{high}$ CD4SP progenitors were also markedly reduced (**Figure 1h-i**). Naïve T cells from *loco* mice had impaired capacity to differentiate into Th1 and Th17 subsets of $CD4^+$ T cells (**Supplementary Figure 2g)**. Likewise, T cells from *loco* mice displayed a 7-fold decrease in IL-10 secreting cells under conditions that induce the differentiation of Type 1 regulatory T (Tr1) cells, that act to restrain the activation of effector immune cells (**Supplementary Figure 2g**). Overall, these data identify a defect in Treg cell differentiation at the earliest stage in the thymus of *loco* mutant mice.

To determine whether the lack of Treg cells in *loco* mutant mice reflected cell intrinsic or cell extrinsic defects, lethally irradiated congenic C57BL/6 (Ly5.1/Ly5.2) F1 mice were reconstituted with T cell-depleted bone marrow cells composed of a 1:1 mixture of *loco* mutant ($Ly5.2^+$) and wt (Ly5.1+) cells (**Supplementary Figure 2c)**. Significant proportions of both wt and *loco* mutant bone marrow-derived myeloid, T and B cells were recovered from the thymus, spleen and lymph nodes (**Supplementary Figure 2d, e**). However, almost all Treg cells in the chimeric animals were of wt origin. This finding indicates that the Treg cell defect in the *loco* mutant mice

is cell intrinsic and not secondary to alterations in other hematopoietic cells or stroma. Furthermore, the *Vav-BCL-2* transgene was dispensable for the phenotype (**Supplementary Figure 2f**), indicating that inhibition of the intrinsic apoptotic pathway does not contribute to the immune defects in *loco* mutant mice.

Non-coding mutations in Card11 cause the* loco *phenotype

The vast majority of the known ENU-induced mutations that cause phenotypes occur within coding regions of genes[33]. Therefore, exome-capture sequencing was performed on DNA extracted from spleen cells from *loco* mutant mice. Comparison to the reference C57BL/6 mouse genome revealed a homozygous single nucleotide variant (SNV) in *Cyp2w1*. SNV Taqman assays revealed that this mutation segregated with the phenotype, with 7/7 of affected mice being homozygous for this mutation versus 0/9 unaffected mice (**Figure 2a**). We noted that, although *Cyp2w1* is not widely expressed in the hematopoietic system, it is in close linkage with the prominent immune-associated gene, *Card11*. The immunological phenotype of mice with loss-of-function *Card11* mutations bear close resemblance to the *loco* mutant mice, with severe reduction of Treg cells, dysregulation of IgD/IgM on B cells and, in some cases, atopic dermatitis (**Figure 1**)[25, 34, 35]. This high similarity prompted us to test whether mutations in *Card11* in linkage with *Cyp2w1*, but missed by the exome sequencing, might actually cause the *loco* phenotype. CARD11 was readily detectable by Western blot analysis in spleen or thymus extracts from wt mice, but this protein was undetectable in cell extracts from the *loco* mutant mice (**Figure 2b**). This finding reveals that the *loco* mutant mice are CARD11-deficient. To find mutations in linkage with *Cyp2w1* that cause the complete loss of CARD11 protein, we conducted whole genome sequencing of DNA from *loco* mutant mice. Three homozygous SNVs were identified in non-coding regions of the *Card11* gene: SNV1 (intron 2) (141,357,417) (T->C), SNV2 (intron 10) (141,371,546) (C->T) SNV3 (intron 20) (141,394,551 (C->A) (**Figure 2c**).

To explore the possibility that one or more of these intronic SNVs causes improper splicing and/or maturation of *Card11* transcripts, we first performed quantitative PCR analysis of cDNA from lymphocytes from wt and *loco* mutant mice. *Card11* transcript could be detected in various immune cell types from *loco* mutant mice at levels 30-65% lower than those in their wt

counterparts (**Figure 2d**). To determine whether splicing defects might cause incomplete transcription of *Card11* in *loco* mutant mice, we performed further qPCR with probes spanning the different exon boundaries throughout the *Card11* gene. Transcripts encoding these regions could be detected (albeit at reduced levels) in immune cells from the *loco* mutant mice. These data indicate that there is no gross truncation of *Card11* mRNA in the *loco* mutant mice (**Figure 2e**). To formally test that the *Card11* mutations detected were responsible for the Treg cell deficiency in the *loco* mutant mice, we took advantage of an independently derived ENU mutant mouse strain with recessive loss-of-function mutation in the *Card11* gene, called *unmodulated*[35]. *Unmodulated* and *loco* mutant mice were intercrossed to produce animals heterozygous for both mutant alleles. Since both are recessive mutations, if the mutation(s) causing the phenotype in *loco* mutant mice resided in the *Card11* gene, we would expect that *loco/unmodulated* double heterozygous mice should have a severe deficit in Treg cell production, similar to homozygous *loco* or *unmodulated* mutant animals. Indeed, 5 out of 5 *loco/unmodulated* double heterozygous mice had a severe deficiency in circulating Treg cells and dysregulated IgM/IgD surface expression on B cells, features normally seen only in the homozygous *loco* or *unmodulated* mutant mice (**Figure 2f)**. Collectively, these data indicate that the immune defects in *loco* mutant mice are caused by non-coding mutation(s) of *Card11* that completely ablate the expression of CARD11.

Treg cell homeostasis in loco mutant mice.

Many studies have characterized defective Treg cell differentiation in adult *Card11*-deficient mice. However, it remains unclear whether this block occurs in early life, whether the peripherally-induced Treg cells respond normally to homeostatic cues *in vivo* and whether these cells are functionally comparable to Treg cells from wt mice. Recent studies have shown that a wave of neonatal Treg cells from the thymus seeds peripheral organs in young mice and that these Treg cells are maintained during adult life[36]. Given that this early postnatal wave of Treg cells emerge under different homeostatic conditions (i.e. lymphopenia), we sought to determine whether they formed the residual Treg cell population detectable in adult *loco* mutant mice. Flow cytometric analysis revealed that the Treg cell deficit was also apparent in the thymus and periphery of 5 day-old *loco* mutant mice (**Figure 3a**). This result indicates that the thymic production of Treg cells in these mice is severely compromised throughout development.

To establish the provenance and functional capacity of the few Treg cells we could detect in the *loco* mutant mice, we performed a deeper phenotypic analysis with cell surface markers of activation (CD44, KLRG1, GITR, CTLA4, CD62L), origin (NRP1) or effector function (ICOS, CTLA4). Importantly, Neuropilin-1 (NRP1) has been reported to be expressed on Treg cells that are thymus-derived, but not on those induced in the periphery from $CD4^+$ conventional T cells[17]. The few Treg cells that could be recovered from the spleen or lymph nodes of *loco* mutant mice had an activation profile comparable to those seen in Treg cells from wt mice (**Figure 3b**). The comparatively lower NRP1 expression in Treg cells found in the *loco* mutant mice supports the notion that these residual cells had been induced in the periphery, a finding that was also suggested by previous studies of other CARD11-deficient mouse strains[37,25]. However, the Treg cells in the spleen and peripheral lymph nodes from the *loco* mutant mice also had decreased expression of ICOS but increased levels of CTLA4 and KLRG1 (**Figure 3c**). We therefore conclude that the *loco* mutant mice have a severe defect in the thymic production of Treg cells but can produce low numbers of induced Treg cells in the periphery that tend to have an effector phenotype. These data reinforce the notion that CARD11 is essential for the induction of thymic Treg cell differentiation throughout life, yet dispensable for conventional CD4SP T cell differentiation and that the low numbers of peripherally-induced Treg cells have an effector phenotype.

To determine whether these peripherally-induced Treg cells in the *loco* mutant mice were capable of responding to IL-2, we administered this cytokine complexed with the anti-IL-2 monoclonal antibody, Jes6-1, a protocol that selectively drives the expansion of cells expressing the high affinity IL-2 receptor, such as Treg cells[19]. Treg cells expanded markedly in the spleen, PLN and MLN of *loco* mutant mice treated with this reagent (**Figure 4a-d**). In terms of the fold increase induced by the IL-2 complexes, the Treg cells in the *loco* mutant mice actually exhibited a greater response compared to the Treg cells in the wt mice (**Figure 4d**). The IL-2/anti-IL-2 antibody complexes expanded Treg cells from the *loco* mutant mice maintained the $NRP1^{low}$, $CTLA4^{low}$, $ICOS^{low}$ phenotype of their resting precursors (**Figure 3c, 4e**). The ability of the peripherally-induced Treg cells from the *loco* mutant mice to expand in response to the IL-2/anti-IL-2 antibody complexes demonstrates that the IL-2 receptor signaling pathway remains intact in

these cells. Hence, defects in this pathway do not explain the Treg cell deficiency seen in the *loco* mutant mice.

Although functional Treg cells from *Card11* mutant mice can be induced *in vitro* from conventional $CD4^+$ T cells[25], the suppressive capacity of the *Card11*-deficient Treg cells induced *in vivo* has not been directly compared to those from wt mice. The substantial expansion of Treg cells induced in the *loco* mutant mice by the IL-2 complexes allowed the isolation of sufficient numbers of these cells for *in vitro* conventional T cell suppression assays. Of note, the IL-2/anti-IL-2 antibody complex-expanded Treg cells from *loco* mutant mice were readily able to suppress the proliferation of wt $CD4^+$ T cells stimulated with anti-CD3/CD28 antibodies, albeit to a slightly lesser extent compared to Treg cells from wt mice (**Figure 4f, g**). These data show that CARD11 is not required for Treg cell responses to IL-2, nor their capacity to mediate suppression of activated conventional T cells.

Discussion

CARD11 is a pivotal protein in lymphocyte differentiation and activation. Numerous *Card11* coding mutations have demonstrated a spectrum of immune pathologies associated with gain- or loss-of-function[38]. The relative abundance of ENU-induced *Card11* mutants is remarkable. Although multiple ENU-induced lesions on the same gene has been observed before (e.g. *Zap70*; [39]), this feature of *Card11* is likely a consequence of the large size of this gene (approximately 127kb) and the striking immunological phenotype that disruption induces. Our study is the first description of a non-coding *Card11* mutation that abolishes expression and presents a novel tool for the study of the regulation of this key immune gene. Although the complementation of the recessive *loco* and *unmodulated* mutant alleles provides compelling evidence that one or more of the three non-coding mutations in the *loco* mutant mice is/are damaging, the mechanism underlying this outcome remains unclear. We did not find evidence for truncation of the *Card11* transcript in cells from the *loco* mutant mice, yet the amounts of mRNA were reduced to approximately one half or one third wt levels. One hypothesis that might explain the reduced *Card11* transcript and absence of CARD11 protein in *loco* mutant mice is that the mutations somehow de-stabilize *Card11* transcripts and prevent translation. An *in silico* analysis did not reveal the introduction of novel splice variants or cryptic miRNA binding sites; therefore, future

studies will be required to identify the mechanisms by which these mutations abrogate CARD11 protein expression.

The profound defect in thymic Treg cell differentiation observed in other *Card11* loss-of-function mutants was reproduced in *loco* mice. Treg cells and their precursors were virtually undetectable in the thymus of *loco* mutant mice and those Treg cells recovered in the periphery were enriched in the mesenteric lymph nodes and lacked expression of the thymic Treg cell marker, NRP1. This defect is thought to reflect the heightened requirement for NF-κB signaling for the production of thymic Treg cells[8]. However, one study suggested that CARD11 directly operates in IL-2R signaling to complete thymic Treg cell differentiation[24]. By contrast, other studies found that the induction of Th1/Th2 and Treg cell differentiation from mature *Card11*-deficient T cells could be induced *in vitro*[25, 37]. These data suggest that some IL-2/IL-2R signaling remains in the absence of CARD11. Our data align with these findings and also show that peripherally-induced Treg cells from *loco* mutant mice readily expand *in vivo* in response to IL-2/anti-IL-2 antibody complexes. One possibility to explain the discrepancies in these studies is that there may be a distinct role for CARD11 in IL-2R signaling in thymocytes versus mature peripheral T cells. Re-imposing IL-2 signaling or survival signals cannot restore thymic Treg cell differentiation[37]. However, these findings might also reflect a requirement for CARD11 in the establishment of IL-2 responsiveness in thymic Treg cell precursors indirectly. Regardless, our data show that, *in vivo*, CARD11 is not absolutely required for Treg cell homeostatic responses to IL-2 and the lack of IL-2 production from conventional cells delimits the peripherally-induced Treg cell compartment[18, 34]. Furthermore, we demonstrate that the expanded Treg cells in the *loco* mutant mice are functional, as they could suppress the proliferation of mitogen stimulated conventional wt $CD4^+$ T cells *in vitro*.

The development of atopic dermatitis in the *loco* mutant mice is curious. This phenotype has only been reported in the *unmodulated* and *king* ENU mutant mouse strains which, in contrast to the complete loss-of-function apparent in *loco* mice, appear to be CARD11 hypomorphs[25, 35]. Whilst studies conducted on *Card11* null mice did not report development of dermatitis, they did not report data on aged animals. It is therefore possible that these mice were not kept long enough for this phenotype to become apparent. Alternatively, it remains possible that *loco*

mutants are in fact CARD11 hypomorphs, despite the fact that we could not detect protein under the Western blot conditions used here. Nevertheless, we speculate that the development of dermatitis in the *loco* mutant mice, like in the *unmodulated* mutant mice, reflects the distinct impact of CARD11-deficiency on Treg *vs* Th2 cells [25]. Furthermore, it is known that Treg cells do not impose the same level of suppression on all effector T cell types[26, 40], therefore such that asymmetric control of Th2 responses may also contribute to the hyper-IgE and dermatitis observed in *loco* mutant mice.

In contrast, some patients with partial loss-of-function mutations in *Card11* develop atopic disease but have normal Treg cells in the blood[41]. In these cases, cell intrinsic defects in conventional T cell activation may be sufficient to drive disease. The apparently normal Treg cell homeostasis in these patients suggests that both thymic Treg cell differentiation and peripheral homeostasis is intact. The latter observation is in accord with our data showing that the IL-2 response and suppressive function of *Card11*-deficient Treg cells is largely normal. Patients with complete loss-of-function *Card11* mutations have severe Treg cell deficiency[42], more akin to the observations in most mouse *Card11* mutants (including *loco* mice). We would posit that impaired thymic Treg cell differentiation is sufficient to explain this deficit.

In conclusion, the *loco* mutant mice provide a novel tool for studying the regulation of CARD11 expression and our data show that CARD11 is dispensable for Treg cell homeostatic responses *in vivo* and suppressive function *in vitro*.

Methods

Mice

Mice were housed in specific pathogen-free conditions at the Australian Phenomics Facility (APF) or the Walter and Eliza Hall Institute (WEHI) Bioservices. All experiments were approved by the Australian National University Animal Ethics and Experimentation Committee or WEHI Animal Ethics Committee. The *Card11*$^{loco/loco}$ strain was derived from C57BL/6 mice treated three times i.p. with 100 mg/kg body weight *N*-ethyl-*N*-nitrosourea at weekly intervals. Mice were maintained on an inbred C57BL/6 background. The Vav-*BCL2*Tg mice were

generated and maintained on an inbred C57BL/6 background[30]. C57BL/6.Ly5.1 mice were obtained from WEHI Bioservices.

Exome enrichment, sequencing, SNV detection and validation.

Exome sequencing and SNVs detection was performed as previously described [43]. Briefly, DNA was extracted from the ear tissue of affected mice, paired-end genomic libraries prepared in technical replicates (Illumina, CA) and exome enrichment performed using the SureSelect Mouse Exome kit (Agilent, CA) following the manufacturer's protocols. Four amplification cycles were performed in the library pre-capture PCR and eight cycles in the post-enrichment amplification. Enriched libraries were diluted to 7-8 pM for cluster generation and sequencing-by-synthesis on an Illumina HiSeq as 100 bp reads. A previously described custom workflow was used to call SNVs [43]. SNVs were validated using Amplifluor assays (Chemicon, CA), with primers designed using the Assay Architect tool (http://serologicals.com/AAA/mainmenu.aspx). Fluorescent intensities were detected using a Fluostar Optima (BMG).

Whole genome sequencing

Genomic DNA was extracted, and a library constructed following the Illumina TruSeq DNA library prep protocol. The library was sequenced by Beijing Genomics Institute (BGI) on an Illumina HiSeq 2000, using 100 bp paired-end reads. The reads were quality-filtered and mapped to the mouse genome reference for C57BL/6J (NCBI version 37.2). SNVs were called using the SAMtools [44] mpileup program and filtered on read depth and quality. The filtered SNVs were visually validated using the Integrated Genomic Viewer (IGV) [45] program.

Flow cytometry

Dissected lymphoid organs were collected in RPMI medium with 25.96 mM HEPES, mashed between frosted glass slides and filtered through 100 micron mesh. Cells ($3x10^6$) were stained with antibody conjugates (see **Immunoconjugates** below) to detect cell surface proteins for 15 min at 4˚C. Cells were then washed in FACS buffer (PBS containing 2% FCS and 0.1% NaN_3) and resuspended in a final volume of 200 μL of FACS buffer containing Propidium Iodide (PI) at a final concentration of 2.5 μg/mL prior to acquiring the data to determine dead cells.

Intra-cellular staining of proteins was conducted using the FOXP3 staining kit (Invitrogen eBiosciences, California). Cell pellets were resuspended in 100 μL of fixation/permeabilization diluent solution (1:4) for 1 h at 4°C and stained with antibodies for 30 min at 4°C. Cells were washed and resuspended in 100 μL FACS buffer. The stained cells were acquired on a Fortessa flow cytometer (BD Biosciences), calibrated with single-color stains for electronic compensation of spectral overlap between fluorochromes. Data were analyzed using Flowjo software (TreeStar).

Antibodies and immunoconjugates

Surface labeling of lymphocyte populations was performed using the following antibodies that were made in the WEHI Monoclonal Antibody Facility, unless otherwise stated: unconjugated anti-mouse CD16/32 FcγR block, anti-CD4 PerCP/Cy5.5 (clone 30-F11, Biolegend, California), anti-CD8 APC/Cy7 or BV650 (clone 53-6.7, Biolegend, California), anti-TCRβ-PE-CY7 (H57.59.1, Biolegend), anti-CD25 BV510 (clone PC61, Biolegend, California), anti-CD44 FITC (clone IM781) or anti-CD44 Alexa Fluor 700 (clone 1M7, Biolegend, California), anti-CD62L APC/Cy7 (clone MEL-14, Biolegend, California), anti-NK1.1 biotin (clone PK136, Biolegend, California), anti-TER119 biotin (TER119), anti-GR1 biotin (clone RB6-8C5), anti-MAC-1 biotin (clone M1-170), anti-B220 biotin (RA3-6B2), anti-PD1 PE (clone 29F.1AI2, Biolegend, California) and anti-CTLA4 APC (clone UC10-4B9, Biolegend, California). Second step labeling to detect biotinylated antibodies was with streptavidin BV786 (Biolegend, California). Intracellular staining was performed with anti-FOXP3 e450 (clone FJK-165, Invitrogen eBioscience, California) and anti-human Ki67 FITC (clone MOPC-21, BD Pharmingen) after fixation and permeabilization with eBioscience FOXP3 staining kit.

Western blotting

Cells from spleens and thymi were lysed with the addition of Laemmli sample buffer. Cell lysates were fractionated with 7% SDS-PAGE and transferred to a nitrocellulose membrane. CARD11 and tubulin were detected by staining with anti-CARD11 (1D12, #4435) and anti-α/β tubulin (#2148) antibodies, respectively.

***In vitro* Treg cell suppression assay**

Single cell suspensions of spleen and lymph nodes (pooled axial and brachial) were mashed and filtered. Splenocyte suspensions were incubated with 2 mL red cell removal buffer (RCRB) for 2 min, underlayed with 1 mL of FCS and washed in KDS/BSS media. Spleen and lymph node cell suspensions were combined and stained with antibody conjugates labeling CD4, CD8, CD25 for 30 min at 4°C and washed. Cells were resuspended with 2.5 μg/mL PI in KDS/BSS and then viable CD4+ conventional T cells or CD4+ Treg cells were purified using an Aria II FACS sorter (BD Biosciences). Cells were washed in KDS/BSS and re-filtered into polypropylene tubes. Conventional T cells were washed with PBS, resuspended in Cell Trace Violet (CTV) solution in 0.1% BSA/PBS at a final concentration of 5 μM for 10 min at 37°C. RPMI complete medium (5 mL) was added to the cells and incubated for 10 min at 4°C to quench the reaction. Cells were then washed at 4°C and resuspended in RPMI complete medium for plating at $1x10^4$/well. Sorted Treg cells were recovered by centrifugation and resuspended in RPMI complete medium with anti-CD3 antibodies (1 μg/mL) and plated at varying cell numbers. Irradiated splenocytes (30 Gy) were used as APCs and plated at $4x10^4$/well in RPMI complete medium. Cells were cultured for 72 h in an incubator set at 37°C with 10% CO_2-in-air. Flow cytometry was performed on a Fortessa (BD Biosciences).

Bone marrow reconstitution experiments

Recipient mice were irradiated with 2 doses of 5.5 Gy 3 h apart prior to injection of donor cells. The hind legs of donor mice were dissected and the bone marrow flushed into cold FACS buffer. Cell suspensions were filtered and centrifuged at 1500 rpm for 5 min at 4°C. Cells were counted and resuspended in sterile PBS and 200 μL (5 million cells) was injected intravenously into the tail vein. The following day, 100 μg anti-Thy1 mAb (clone T24) was administered intraperitoneally to deplete residual host T cells.

***In vivo* IL-2/anti-IL-2 antibody complex administration**

IL-2/IL-2 antibody complexes were prepared and administered according to[19]. Briefly, the complexes were prepared at a concentration of (1 μg IL-2: 5 μg anti-IL-2 antibody, Peptrotech) and incubated in a 37°C water-bath for 30 min. For each injection, 7 μL of the complex mixture was diluted in PBS to a final volume of 200 μL to be injected per mouse i.p.. Recipient mice between 8-12 weeks of age were injected with IL-2:anti-IL-2 (JES6-1, Bio X cell) complexes or

diluent (PBS) on days 0, 1 and 2. On day 5, mice were euthanized and thymocytes, splenocytes and lymphocytes from LNs isolated for flow cytometric analysis of conventional T cells and Treg cells.

Quantitative real-time PCR analysis

Cells or tissues were suspended in 500 µL of TRIZOL, then 100 µL of chloroform was added and samples shaken vigorously for approximately 15 sec followed by incubation at room temperature for 2-3 min. Samples were then centrifuged at 12,000 x g at 4^{o}C for 15 min and the aqueous (top layer) was carefully transferred to a new 1.5 mL Eppendorf tube. The samples were kept on ice from this step onward unless otherwise stated. The aqueous phase containing the RNA was transferred to a new tube and 1 µL of Glycoblue was added to each sample, flicked, spun and kept on ice. To precipitate the RNA, 250 µL of ice-cold Isopropanol was added and samples incubated at 80^{o}°C for 1 h. After incubation, the samples were thawed on ice and centrifuged at 12,000 x g at 4^{o}°C for 20 min. The supernatant was removed, washed with 500 µL of 75% cold ethanol and centrifuged at 7,000 x g at 4^{o}°C for 15 min. The ethanol was carefully removed and the samples were air dried at RT for 10 min. The RNA pellet was then resuspended in 12.5-15 µL nuclease-free water and total RNA was quantified using a NanoDrop (Thermo Fischer Scientific). RNA was reverse transcribed into cDNA using 8 µL of RNA sample in a final volume of 20 µL using Super Script III First Strand CDNA Synthesis Kit (Invitrogen, California) and Oligo(dT). The freshly prepared cDNA was subsequently diluted to 1:10 and the qRT-PCR reaction was set up using 1 µL of diluted cDNA, 5 µL of TaqMan Master Mix (Applied Biosystems, California), 0.5 µL of the Taqman Primer and 3.5 µL water. The procedure was performed using the ABI 7900 (Applied Biosystems, California) using 384-well Clear Optical Reaction Plates with Barcode (Applied Biosystems) and Microamp Optical Adhesive Film (Applied Biosystems). Each sample was run in triplicate and the expression levels of *Card11* were calculated using $2^{\Delta\Delta}$Ct method using *Hmbs* as a housekeeping gene.

Measurement of serum IgE

Serum IgE (1:10 dilution) was measured by ELISA using 2 µg/ml rat anti-mouse IgE antibodies (Southern Biotech, clone 23G3) as a capture reagent and developed with 1:500 mouse Ig isotype-specific goat anti-mouse IgE (Fc specific) antibodies conjugated to horseradish peroxidase

(Nordic MUBio). The capture reagent was applied overnight at 4°C, sera were applied for 4 hours at room temperature and ELISA plates were developed in the dark for 45 min at room temperature. IgE isotype monoclonal anti-dinitrophenyl antibody produced in mouse, IgE isotype (Sigma, MO, clone SPE-7) were used as standards.

T cell polarisation assay

Flat-bottom 96-well plates were coated with 10 μg/mL of anti-CD3 antibodies diluted in PBS and incubated overnight at 4°C. Spleens were harvested and subjected to $CD4^+$ T cell enrichment using Automacs LS columns (Miltenyi), and further enriched for $CD4^+$ $CD62^{hi}$ T cells using an Aria II FACS sorter (BD Biosciences). Cells (15,000) were seeded per well and resuspended in medium containing the appropriate cytokine mix then incubated at 37°C and 5% CO_2. Half of the culture mix was harvested at 72 hours and the remainder of the culture at 120 hours. Upon harvest cells were stimulated with PMA 50mg/ml, Ionomycin 0.5mg/ml and Golgiplug/Golgistop (1:500) for 3 hours at 37°C and 5% CO_2. Culture conditions: Th0 (1.5ug/ml α-CD28), Th17 (1.5ug/ml α-CD28; 10ug/ml α-IFN-γ; 10ug/ml α-IL-4; 5ng/ml TGFβ; 20ng/ml IL-6), Th1 (1.5ug/ml α-CD28; 10ug/ml α-IL-4; 10ng/ml IL-12), Tr1 (1.5ug/ml α-CD28; 5ng/ml TGFβ; 100ng/ml IL-27). Surface labeling of lymphocyte populations was performed using the following antibodies that were made in the WEHI Monoclonal Antibody Facility, unless otherwise stated: unconjugated anti-mouse CD16/32 FcγR block, anti-CD4 PerCP/Cy5.5 (clone 30-F11, Biolegend), anti-CD8 BV650 (clone 53-6.7, Biolegend), anti-TCRβ-PE-CY7 (H57.59.1, Biolegend), anti-CD25 BV510 (clone PC61, Biolegend). Intracellular staining was performed with Invitrogen eBiosciences FOXP3 staining kit. Antibodies detected: IFN-γ (clone XMG1.2, BD), IL-17A (clone TC11-18H10, BD), IL-10 (clone JES5-16E3, BD), Lag3 (clone C9B7W, eBioscience), TNFα (MP6-XT22 Biolegend), FOXP3 (FJK-16s, eBioscience). Flow cytometry was performed on a Fortessa (BD Biosciences).

Statistical analysis

Statistical comparisons were made using one-way ANOVA with multiple comparisons with Prism v.6.0 (GraphPad). *P-values* <0.05 were considered to indicate a statistically significant difference.

Figure Legends

Figure 1. Identification of the ENU-induced mutant mouse *loco*.

(**a**) Representative FACS profiles of CD4 *vs* CD25 expression on $CD4^+$ T cells from blood lymphocytes from wt or putative mutant (putant) mice. (**b**) The mean percentage (±SEM) of $CD4^+$ $CD25^+$ blood lymphocytes from mice in the screen that identified the *loco* mutant mouse. Each dot represents the data from one mouse and the dashed line shows -3SD. Other panels show mean percentages of $CD4^+CD25^+$ (top right), $CD19^+$ (bottom left) and $CD4^+$ (bottom right) blood lymphocytes from wt and homozygous *loco* mutant mice. (**c**) Representative FACS profiles of expression of IgD *vs* IgM on spleen cells of wt or *loco* mutant mice. (**d**) Representative image of the atopic dermatitis that develops in the *loco* mutant mice (a 162 day-old mouse is shown) (**e**) H&E staining of affected skin from a *loco* mutant mice. (**f**) Curve of dermatitis-free survival of wt (n=15) and *loco* mutant mice (n=36). (**g**) Serum IgE of wt and homozygous *loco* mutant mice as measured by ELISA and expressed as relative absorbance. (**h**) Representative FACS profiles of FOXP3 *vs* CD25 expression gated on $CD4^+$ T cells from the organs indicated in wt or *loco* mutant mice. Numbers indicate percentages of cells gated. Peripheral lymph nodes were pooled: axial, brachial and inguinal. (**i**) Representative FACS profiles of CD4 *vs* CD8 expression (total thymocytes, left panels), GITR *vs* CD4 (CD4SP, middle) and FOXP3 *vs* CD25 (CD4SP, right) on thymocytes from wt and *loco* mutant mice. Numbers indicate percentages of cells gated. (**j**) Bar graphs of the mean percentages (±SEM) of FOXP3+ Treg cells in $CD4^+$ lymphocytes from the organs indicated in wt or *loco* mutant mice. n=5 per group. (**k**) Bar graph comparing mean percentage (±SEM) of $GITR^+$ or $CD25^+$ cells among CD4SP thymocytes. Data in a, c, e, g are representative of 2-4 experiments performed with n = 3-5 mice per group. * $P<0.05$, *** $P<0.001$, **** $P<0.0001$ Student's t-test.

Figure 2. Non-coding SNVs in the *Card11* locus cause the *loco* phenotype.

(**a**) Graph of data from Taqman assay for the *Cyp2w1* single nucleotide variant (SNV). The phenotype of mice affected or unaffected by the low proportion of $CD4^+CD25^+$ cells and

IgD/IgM dysregulation in circulating lymphocytes is overlaid with the SNV typing data. (**b**) Western blot analysis of lysates from spleen cells or thymocytes isolated from wt or *loco* mutant mice. The blot was probed for CARD11 and Tubulin (loading control). (**c**) Table and schematic representation of the 3 *Card11* SNVs identified by whole genome sequencing of *loco* mutant cells. The position and nature of the mutations are shown. Red diamonds denote the location of the 3 mutations in relation to gene exons indicated by the numbers (not to scale). (**d**) Bar graphs of mean (±SEM) mRNA transcript levels of *Card11* in organs or cells from wt and *loco* mutant mice. Data were normalized to housekeeping gene HMBS, and expressed relative to the signal in the respective tissues from wt mice. (**e**) Bar graphs of mean (±SEM) mRNA transcript levels of *Card11* in wt and *loco* mutant mice across the indicated exons of the gene. Data are representative of 3 experiments, with one mouse per group per experiment. *** $P < 0.001$, **** $P < 0.0001$ Student's t-test. (**f**) Representative FACS profiles comparing surface expression of IgD *vs* IgM (left plots) or FOXP3 vs CD25 (right plots, gated on $CD4^+$ T cells) on spleen cells of wt and *unmodulated*/*loco* double heterozygote mutant mice. Table of the genotype and phenotype of F1 progeny from intercrosses of wt/*loco* and wt/*unmodulated* mice.

Figure 3. Thymic Treg cell deficiency in neonatal and adult *loco* mutant mice.

(**a**) Representative FACS profiles of CD4 *vs* FOXP3 expression on $CD4^+$ T cells from the indicated organs from wt or *loco* mutant mice. (**b**) Representative FACS profiles comparing surface expression of activation markers on $CD4^+$ $Foxp3^+$ Treg cell populations from the indicated organs from wt or *loco* mutant mice. (**c**) Representative histograms comparing surface marker expression on $CD4^+FOXP3^+$ cells from the indicated organs from wt (solid gray) and *loco* mutant (black lines) mice. Data are representative of 1-3 experiments performed with *n*=3-5 per group. Numbers indicate percentages of cells gated.

Figure 4. IL-2/IL-2 antibody complex-induced expansion of *Card11*-deficient Treg cells from *loco* mutant mice.

(**a**) Representative FACS profiles of Treg cell populations in the organs indicated from wt (top panels) or *loco* mutant mice (bottom panels) that had received PBS or IL-2:anti-IL-2 antibody complexes. N=3 per group. (**b**) Bar graphs of mean percentage (±SEM) or (**c**) mean splenic Treg cell numbers (±SEM) across treatment groups indicated. (**d**) Bar graph of the mean fold increase

in Treg cell numbers between IL-2:anti-IL-2 antibody complex *vs* PBS treatments in wt and *loco* mutant mice in the organs indicated. (**e**) Representative histograms of Treg cell surface marker expression in wt IL-2:anti-IL-2 antibody complex injected (black line), wt PBS injected (black dotted line) and *loco* mutant IL-2:anti-IL-2 antibody complex injected mice (solid grey line). (**f**) Representative histograms of wt $CD4^+$ T cells CTV dilution following anti-CD3 antibody stimulation and culture with various ratios of IL-2:anti-IL-2 antibody complex expanded Treg cells from wt or *loco* mutant mice. Numbers denote the proportions of divided cells. (**g**) Graph of mean Treg cell suppression of conventional $CD4^+$ T cell proliferation across various concentrations of IL-2:anti-IL-2 antibody complex expanded Treg cells from wt or *loco* mutant mice. Data are representative of 1-3 experiments performed with 1-5 mice per group. * *P <0.05,** P <0.01,*** P <0.005, **** P <0.001;* Student's t-test.

Supplementary figure 1. **Histological analysis of organs from *loco* mutant mice.**
H&E stained sections of the indicated organs taken from wt or *loco* mutant mice demonstrate little evidence of lymphocytic infiltration or pathology. Scale bar= 500μM

Supplementary figure 2. **T cell differentiation and homeostasis in *loco* mutant mice.**
(**a**) Bar graph of mean percentages of $CD4^+$ T cells (±SEM) among lymphocytes in the indicated organs from wt or *loco* mutant mice. (**b**) Representative FACS profiles of CD25 *vs* CD44 expression on lineage-negative $CD4^-CD8^-$ thymocytes from wt or *loco* mutant mice. (**c**) Experimental schematic for construction of mixed bone marrow chimeras. (**d**) Bar graphs showing the mean percentage of chimerism derived from wt (black bars) or *loco* (grey bars) progenitor derived cells in the T cell subsets indicated. (**e**) Representative FACS profiles of CD4 *vs* FOXP3 expression on lymphocytes from wt (top panels) or *loco* mutant mice (bottom panels) in the organs indicated. Numbers indicate the percentages of conventional $CD4^+$ T cells and $CD4^+FOXP3^+$ Treg cells. (**f**) Graph comparing the percentages of $CD4^+CD25^+$ Treg cells among circulating $CD4^+$ T cells in mice of the indicated genotypes. Each dot is representative of one mouse and the mean (±SEM) is shown. Statistical analysis by Student's t-test, *** *P <0.001*. **(g)** Representative FACS profiles of purified $CD4^+$ $CD62L^{hi}$ T cells cultured under T-cell polarising conditions for 72 hours from wt (top panels) or *loco* mutant mice (bottom panels). Numbers indicate percentages of populations gated.

Acknowledgements:

Antonia N. Policheni is supported by a Cancer Council Victoria Postdoctoral Fellowship. This work was also supported by Cancer Council of Victoria Grants-in-Aid to Daniel H.D. Gray (1146518 & 1102104), Australian NHRMC Project Grants (1145888 & 1121325) to Daniel H.D. Gray, NHMRC program grant #1016701 Andreas Strasser and Leukemia and Lymphoma Society of America Specialized Center of Research (SCOR) grant #7001-13 to Andreas Strasser, Cancer Australia and Cancer Council New South Wales project grant #1047672 to L.A. O'Reilly. Gabrielle T. Belz is supported by an Australian NHMRC Senior Principal Research Fellowship (1135898). Daniel H.D. Gray is supported by an Australian NHMRC RD Wright Fellowship (1090236). Andreas Strasser is supported by an Australian NHMRC Senior Principal Research Fellowship (1020363). This work was made possible through Victorian State Government Operational Infrastructure Support and Australian Government NHMRC IRIISS. Liz Milla's work was supported by Melbourne Bioinformatics (VLSCI), The University of Melbourne. The authors gratefully acknowledge Hayley Marks, Faye Dabrowski and Stephanie O'Connor for mouse husbandry, Bruno Helbert and Stephanie Fennell for genotyping, Charis Teh, Alissa Robbins, Lisa Mielke and Tom Sidwell for the provision of technical advice and reagents.

References.

1. Brunkow ME, Jeffery EW, Hjerrild KA*, et al.* Disruption of a new forkhead/winged-helix protein, scurfin, results in the fatal lymphoproliferative disorder of the scurfy mouse. Nat Genet. 2001;**27**:68-73.

2. Bennett CL, Christie J, Ramsdell F*, et al.* The immune dysregulation, polyendocrinopathy, enteropathy, X-linked syndrome (IPEX) is caused by mutations of FOXP3. Nat Genet. 2001;**27**:20-21.

3. Wildin RS, Ramsdell F, Peake J*, et al.* X-linked neonatal diabetes mellitus, enteropathy and endocrinopathy syndrome is the human equivalent of mouse scurfy. Nat Genet. 2001;**27**:18-20.

4. Chatila TA, Blaeser F, Ho N*, et al.* JM2, encoding a fork head-related protein, is mutated in X-linked autoimmunity-allergic disregulation syndrome. J Clin Invest. 2000;**106**:R75-81.

5. Bennett CL, Ochs HD. IPEX is a unique X-linked syndrome characterized by immune dysfunction, polyendocrinopathy, enteropathy, and a variety of autoimmune phenomena. Curr Opin Pediatr. 2001;**13**:533-538.

6. Fontenot JD, Gavin MA, Rudensky AY. Foxp3 programs the development and function of CD4+CD25+ regulatory T cells. Nat Immunol. 2003;**4**:330-336.

7. Hori S, Nomura T, Sakaguchi S. Control of regulatory T cell development by the transcription factor Foxp3. Science. 2003;**299**:1057-1061.

8. Josefowicz SZ, Lu LF, Rudensky AY. Regulatory T cells: mechanisms of differentiation and function. Annu Rev Immunol. 2012;**30**:531-564.

9. Sakaguchi S, Yamaguchi T, Nomura T*, et al.* Regulatory T cells and immune tolerance. Cell. 2008;**133**:775-787.

10. Xing Y, Hogquist KA. T-cell tolerance: central and peripheral. Cold Spring Harbor perspectives in biology. 2012;**4**.

11. Liston A, Gray DH. Homeostatic control of regulatory T cell diversity. Nat Rev Immunol. 2014;**14**:154-165.

12. Lio CW, Hsieh CS. A two-step process for thymic regulatory T cell development. Immunity. 2008;**28**:100-111.

13. Tai X, Cowan M, Feigenbaum L*, et al.* CD28 costimulation of developing thymocytes induces Foxp3 expression and regulatory T cell differentiation independently of interleukin 2. Nat Immunol. 2005;**6**:152-162.

14. Tai X, Erman B, Alag A*, et al.* Foxp3 transcription factor is proapoptotic and lethal to developing regulatory T cells unless counterbalanced by cytokine survival signals. Immunity. 2013;**38**:1116-1128.

15. Hu DY, Wirasinha RC, Goodnow CC*, et al.* IL-2 prevents deletion of developing T-regulatory cells in the thymus. Cell Death Differ. 2017;**24**:1007-1016.

16. Mahmud SA, Manlove LS, Schmitz HM*, et al.* Costimulation via the tumor-necrosis factor receptor superfamily couples TCR signal strength to the thymic differentiation of regulatory T cells. Nat Immunol. 2014;**15**:473-481.

17. Bilate AM, Lafaille JJ. Induced CD4+Foxp3+ regulatory T cells in immune tolerance. Annu Rev Immunol. 2012;**30**:733-758.

18. Amado IF, Berges J, Luther RJ*, et al.* IL-2 coordinates IL-2-producing and regulatory T cell interplay. J Exp Med. 2013;**210**:2707-2720.

19. Webster KE, Walters S, Kohler RE*, et al.* In vivo expansion of T reg cells with IL-2-mAb complexes: induction of resistance to EAE and long-term acceptance of islet allografts without immunosuppression. J Exp Med. 2009;**206**:751-760.

20. Levine AG, Arvey A, Jin W*, et al.* Continuous requirement for the TCR in regulatory T cell function. Nat Immunol. 2014;**15**:1070-1078.

21. Vahl JC, Drees C, Heger K*, et al.* Continuous T cell receptor signals maintain a functional regulatory T cell pool. Immunity. 2014;**41**:722-736.

22. Bedsaul JR, Carter NM, Deibel KE*, et al.* Mechanisms of Regulated and Dysregulated CARD11 Signaling in Adaptive Immunity and Disease. Front Immunol. 2018;**9**:2105.

23. Ruland J, Duncan GS, Wakeham A*, et al.* Differential requirement for Malt1 in T and B cell antigen receptor signaling. Immunity. 2003;**19**:749-758.

24. Lee AJ, Wu X, Cheng H*, et al.* CARMA1 regulation of regulatory T cell development involves modulation of interleukin-2 receptor signaling. J Biol Chem. 2010;**285**:15696-15703.

25. Barnes MJ, Krebs P, Harris N*, et al.* Commitment to the regulatory T cell lineage requires CARMA1 in the thymus but not in the periphery. PLoS Biol. 2009;**7**:e51.

26. Altin JA, Tian L, Liston A*, et al.* Decreased T-cell receptor signaling through CARD11 differentially compromises forkhead box protein 3-positive regulatory versus T(H)2 effector cells to cause allergy. J Allergy Clin Immunol. 2011;**127**:1277-1285 e1275.

27. Dadi H, Jones TA, Merico D*, et al.* Combined immunodeficiency and atopy caused by a dominant negative mutation in caspase activation and recruitment domain family member 11 (CARD11). J Allergy Clin Immunol. 2018;**141**:1818-1830 e1812.

28. Wang L, Ni X, Covington KR*, et al.* Genomic profiling of Sezary syndrome identifies alterations of key T cell signaling and differentiation genes. Nat Genet. 2015;**47**:1426-1434.

29. Jeon MS, Atfield A, Venuprasad K*, et al.* Essential role of the E3 ubiquitin ligase Cbl-b in T cell anergy induction. Immunity. 2004;**21**:167-177.

30. Ogilvy S, Metcalf D, Print CG*, et al.* Constitutive Bcl-2 expression throughout the hematopoietic compartment affects multiple lineages and enhances progenitor cell survival. Proc Natl Acad Sci U S A. 1999;**96**:14943-14948.

31. Egle A, Harris AW, Bath ML*, et al.* VavP-Bcl2 transgenic mice develop follicular lymphoma preceded by germinal center hyperplasia. Blood. 2004;**103**:2276-2283.

32. Strasser A, Whittingham S, Vaux DL*, et al.* Enforced BCL2 expression in B-lymphoid cells prolongs antibody responses and elicits autoimmune disease. Proc Natl Acad Sci U S A. 1991;**88**:8661-8665.

33. Hoyne GF, Goodnow CC. The use of genomewide ENU mutagenesis screens to unravel complex mammalian traits: identifying genes that regulate organ-specific and systemic autoimmunity. Immunol Rev. 2006;**210**:27-39.

34. Hara H, Wada T, Bakal C*, et al.* The MAGUK family protein CARD11 is essential for lymphocyte activation. Immunity. 2003;**18**:763-775.

35. Jun JE, Wilson LE, Vinuesa CG*, et al.* Identifying the MAGUK protein Carma-1 as a central regulator of humoral immune responses and atopy by genome-wide mouse mutagenesis. Immunity. 2003;**18**:751-762.

36. Yang S, Fujikado N, Kolodin D*, et al.* Immune tolerance. Regulatory T cells generated early in life play a distinct role in maintaining self-tolerance. Science. 2015;**348**:589-594.

37. Molinero LL, Yang J, Gajewski T*, et al.* CARMA1 controls an early checkpoint in the thymic development of FoxP3+ regulatory T cells. J Immunol. 2009;**182**:6736-6743.

38. Turvey SE, Durandy A, Fischer A*, et al.* The CARD11-BCL10-MALT1 (CBM) signalosome complex: Stepping into the limelight of human primary immunodeficiency. J Allergy Clin Immunol. 2014;**134**:276-284.

39. Siggs OM, Miosge LA, Yates AL*, et al.* Opposing functions of the T cell receptor kinase ZAP-70 in immunity and tolerance differentially titrate in response to nucleotide substitutions. Immunity. 2007;**27**:912-926.

40. Tian L, Altin JA, Makaroff LE*, et al.* Foxp3(+) regulatory T cells exert asymmetric control over murine helper responses by inducing Th2 cell apoptosis. Blood. 2011;**118**:1845-1853.

41. Ma CA, Stinson JR, Zhang Y*, et al.* Germline hypomorphic CARD11 mutations in severe atopic disease. Nat Genet. 2017;**49**:1192-1201.

42. Stepensky P, Keller B, Buchta M*, et al.* Deficiency of caspase recruitment domain family, member 11 (CARD11), causes profound combined immunodeficiency in human subjects. J Allergy Clin Immunol. 2013;**131**:477-485 e471.

43. Andrews TD, Whittle B, Field MA*, et al.* Massively parallel sequencing of the mouse exome to accurately identify rare, induced mutations: an immediate source for thousands of new mouse models. Open Biol. 2012;**2**:120061.

44. Li H, Handsaker B, Wysoker A*, et al.* The Sequence Alignment/Map format and SAMtools. Bioinformatics. 2009;**25**:2078-2079.

45. Thorvaldsdottir H, Robinson JT, Mesirov JP. Integrative Genomics Viewer (IGV): high-performance genomics data visualization and exploration. Brief Bioinform. 2013;**14**:178-192.

Figure 1

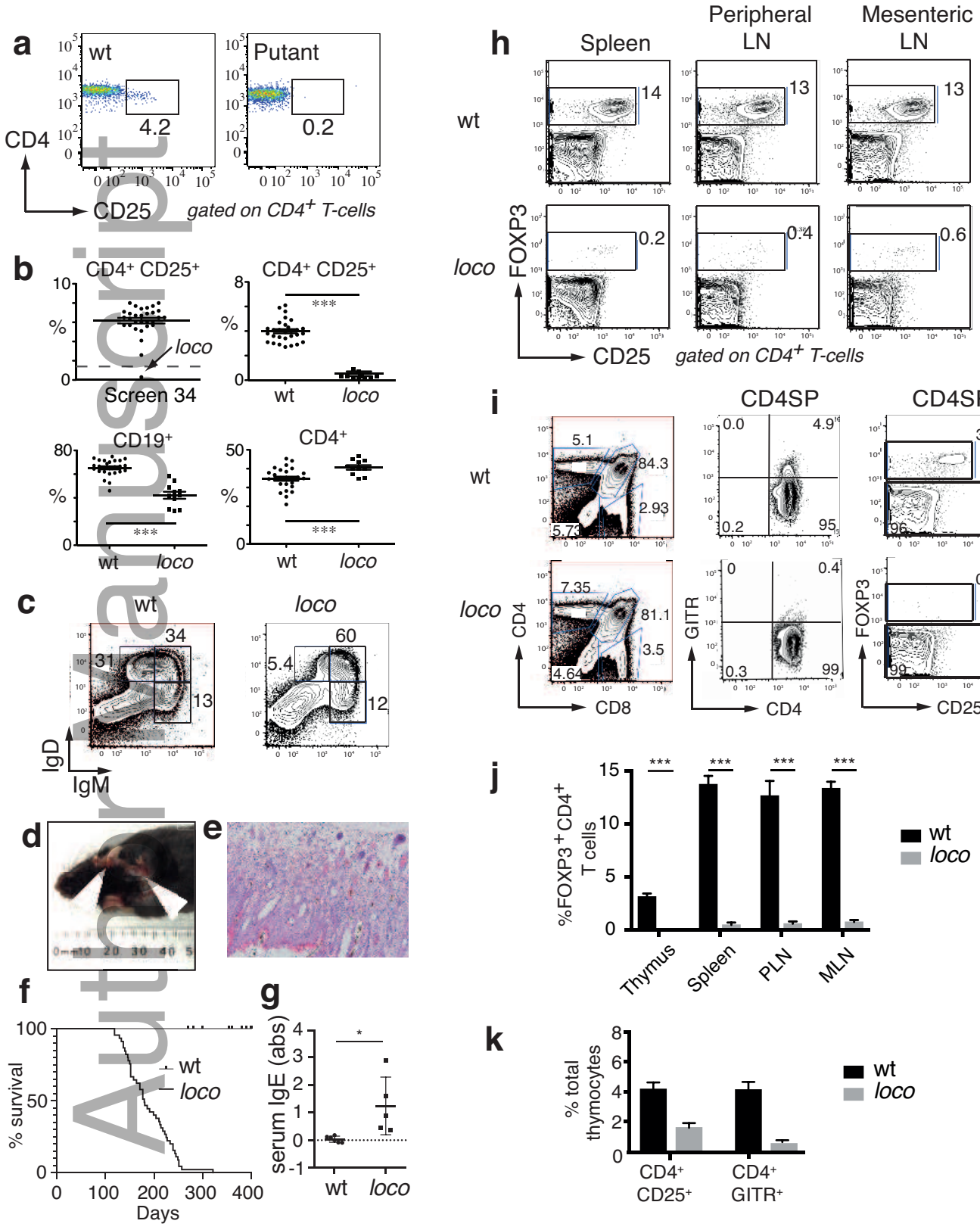

imcb_12268_f1.eps

Figure 2

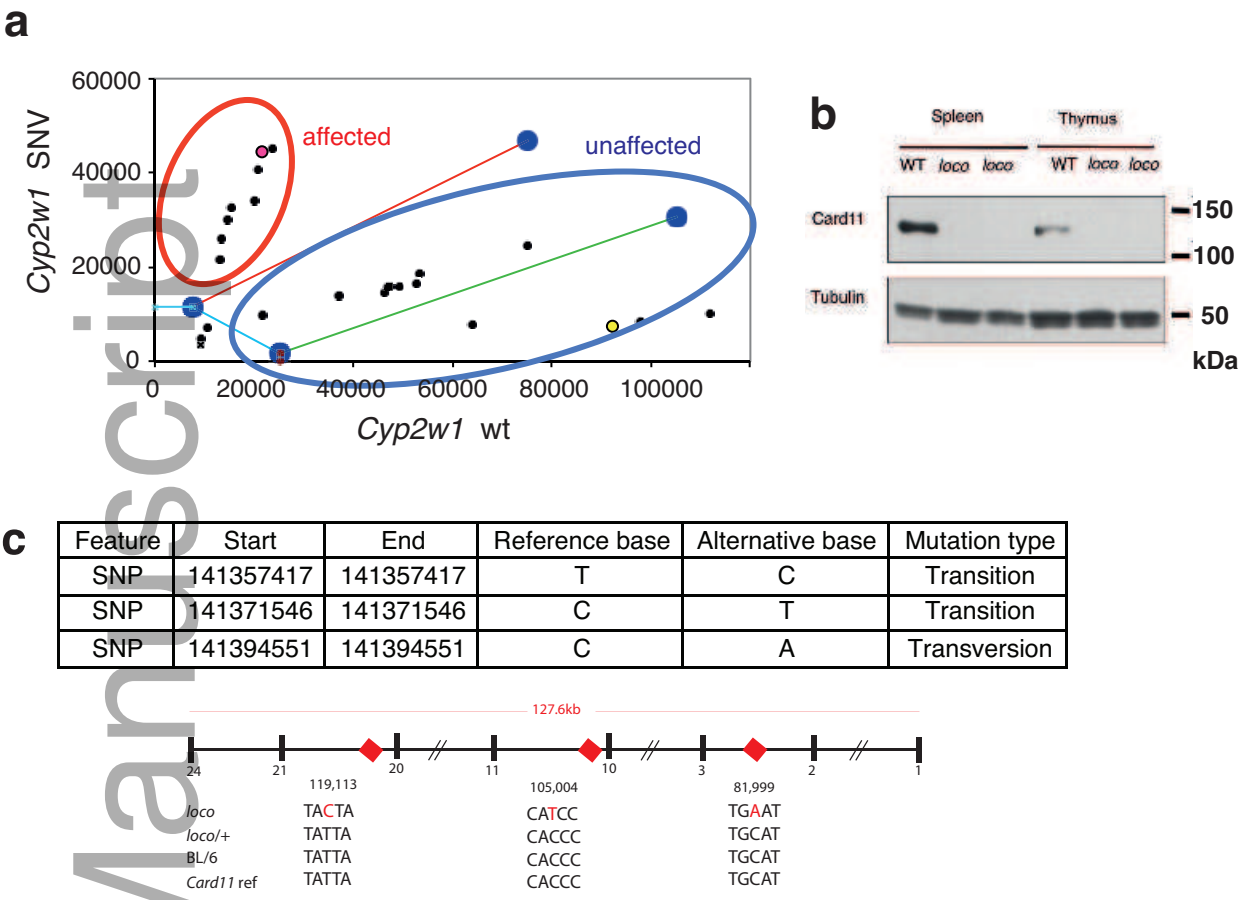

Feature	Start	End	Reference base	Alternative base	Mutation type
SNP	141357417	141357417	T	C	Transition
SNP	141371546	141371546	C	T	Transition
SNP	141394551	141394551	C	A	Transversion

Genotype	Phenotype	
	Unaffected	Affected
wt/wt	5	0
loco/wt	4	0
unmod/wt	1	0
loco/unmod	0	5

Figure 3

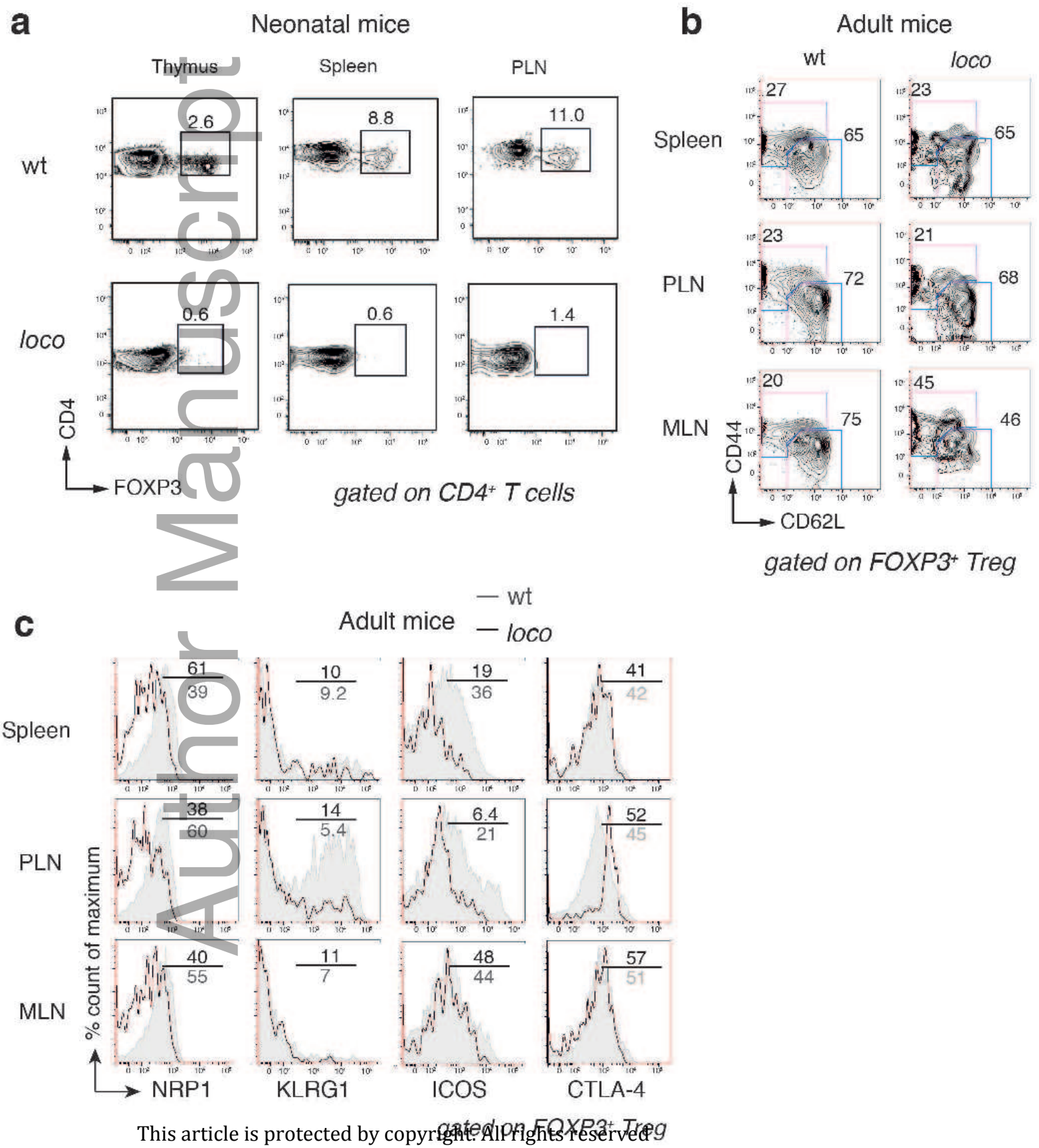

imcb_12268_f3.eps